Layer-KKR theory of negative-ion formation in adsorbed molecules

P. J. Rous
Department of Physics, University of Maryland Baltimore County, Baltimore, Maryland 21228
(Received 30 June 1995)

We present a computational approach for the calculation of the lifetime, energy, and cross sections for negative-ion formation in adsorbed molecules that is based upon a layer-Kohn-Korringa-Rostoker theory. This calculation employs a multiple scattering theory of resonance electron scattering at surfaces in which the substrate scattering is fully incorporated. This method allows the proper treatment of the unoccupied electronic structure of the substrate and its effect upon the lifetime and energy of adsorbate negative ions.

I. INTRODUCTION

An important type of resonant electronic excitation at surfaces is the formation of molecular negative ions.[1] Negative-ion formation is strongly coupled to a variety of dynamical processes at the gas-solid interface[2–4] and is known to be responsible for the resonant enhancement of vibrational excitation observed in high-resolution electron energy-loss spectroscopy (HREELS),[5–13] dissociative attachment,[3] and electron-stimulated desorption.[14] More recent studies have revealed the importance of electron-molecule interactions in surface photochemistry,[15–17] molecular beam scattering,[5,18,19] and dissociative molecular adsorption,[20,21] where the electrons originate in the substrate.

The formation of a molecular negative ion via electron impact can be considered as the temporary occupation by a probe electron of an empty or partially occupied molecular orbital of the host molecule.[22,23] Alternatively, one may view the formation of a negative ion as an electron scattering resonance in which the incident electron is temporarily trapped by the molecule. In the case of a shape resonance, the negative ion is formed by, and decays by, tunneling through the centrifugal barrier. From this scattering viewpoint, the fundamental properties of resonant states in molecules may be considered to be the lifetime of the negative ion, its energy relative to the vacuum level, the symmetry of the resonant state, and its elastic and inelastic cross sections.

A key issue in the fundamental understanding of negative-ion formation at surfaces is how these resonance properties of the free molecule are changed when the molecule is adsorbed at a surface. In principle, the lifetime, energy, cross sections, and symmetry of the molecular negative ion can be altered by the interaction of the resonant state with the substrate. While each of these resonance properties is, in principle, accessible experimentally to HREELS, they cannot be measured directly. Of particular note is the determination of the resonance lifetime from experimental HREELS data, since there is no direct method which allows extraction of the lifetime from the measured resonance profile. For the free molecule, the width of the resonance peak may be related to the inverse of the intrinsic resonance lifetime. While the absence of fine structure in the resonance profile of adsorbates is often taken as an indication of reduced lifetime,[24,25] inelastic processes occurring at the surface may also significantly broaden the observed resonance width of adsorbed molecules. The distinction between a true change in the intrinsic lifetime of the negative ion and a change in the width resonance profile caused by experimental broadening is of critical importance: A change in the trapping time of the probe electron (the *intrinsic* lifetime) would strongly alter the dynamical properties of the adsorbed molecule while resolution broadening is a consequence of the experimental measurement has no such dynamical implications.

It is within this context that the development of a quantitatively useful theory of resonance formation assumes a particular importance. Until recently, all theoretical models of resonance electron scattering, which treated explicitly the issue of the resonance lifetime and energy, employed simple models of the surface potential and parametrization of the molecular scattering. The work of Gerber and Herzenberg[26] and, more recently, Teillet-Billy and co-workers[27,28] and Rous[29] have considered only the screening of the molecular ion by a structureless metallic substrate. These theories rely exclusively upon models of the surface in which the (uncorrugated) substrate potential is represented as a region of constant potential matched onto a classical image potential. The crystalline nature of the substrate was neglected. Nevertheless, these models qualitatively reproduced the observed lifetime and energy of the $^2\Pi_g$ shape resonance in N_2 physisorbed on Ag and predict a monotonic reduction of the energy and lifetime of the negative ion as the molecule approaches the surface. This has led to the adoption of a simple physical picture of the distortion of resonant states by adsorption, originally put forward by Gerber and Herzenberg.[26] The induced image charge shifts the resonance energy downwards relative to the vacuum level. The breaking of the molecular symmetry by the substrate causes the reduction of the resonance lifetime by enabling the pure resonant state to couple into otherwise forbidden partial waves through which the trapped electron escapes through a lower centrifugal barrier.

The ingredient absent from prior theories of resonance electron scattering at surfaces is a quantitative treatment of the interaction of the resonant state with the unoccupied electronic structure of the substrate. Prior theories have considered only the screening of the negative ion by the metallic substrate, and neglected the alteration of the electronic states in the vicinity of the molecule by multiple electron scattering in the substrate. In this paper, we describe the theory and computational implementation of a layer-Kohn-Korringa-

Rostoker (LKKR) calculation of negative-ion formation at surfaces which incorporates, explicitly, the interaction of the probe electron with the unoccupied electronic structure of the substrate.

In this paper, we confine our presentation to the theoretical and computational details of the layer-KKR method. Applications of this method to the calculation of the resonance properties of specific surface-molecule systems can be found elsewhere.[30–34] The organization of the paper is as follows: In Sec. II we discuss the theoretical and computational basis of the layer-KKR theory of resonance scattering in weakly bound adsorbates. In Sec. II A we introduce the scattering matrix $T(E)$. Section II B describes our model of the electron-molecule interaction potential and in Sec. II C we discuss the multiple scattering representation of the probe electron wave function. In Sec. II D we present the theory of electron scattering by adsorbates and describe our treatment of the surface barrier potential (II E) and the substrate (II F). In Sec. II G we discuss and compare several numerical methods for the location of the resonance poles. Section II H describes the numerical treatment of the substrate Brilluoin-zone integrals. The general nature of the substrate scattering matrix S and its relationship to the lifetime and energy of adsorbates is discussed in Sec. III. Concluding remarks, including a brief discussion of the limitations of the present implementation of the layer-KKR theory, are made in Sec. IV.

II. THEORY AND COMPUTATIONAL APPROACH

A. The surface-molecule scattering matrix

Our approach to the calculation of the resonance properties of adsorbates is to compute the energy-resolved scattering matrix $T(E)$ of the surface-molecule system. The resonances of the adsorbed molecule correspond to the poles of T that occur in the lower half of the complex energy plane $E=E_r-i(\Gamma/2)$. Then E_r is the energy of the resonance and Γ is the resonance width. Γ is related to the inverse of the resonance lifetime τ_R,

$$\tau_R=\frac{1}{\Gamma}. \tag{1}$$

When expressed in an angular momentum basis, the scattering matrix $T(E_r)$ yields the (differential) cross section for resonance formation.

The scattering matrix is obtained by solving the Schrödinger equation in which the probe electron and target molecule are represented by a wave function Ψ that is an eigenfunction of the full Hamiltonian $\mathscr{H}$ for nuclear coordinates $\mathbf{R}$ and the molecular center of mass location $\mathbf{R}_M$,

$$\mathscr{H}=-\tfrac{1}{2}\nabla_r^2+H_m(\mathbf{R})+V(\mathbf{r},\mathbf{R},\mathbf{R}_M). \tag{2}$$

Here, $\mathscr{H}$ is written in terms of the kinetic energy of the probe electron, the Hamiltonian of the target molecule, H_m, and the full potential, V, experienced by the scattering electron at position $\mathbf{r}$ due to both the electron-molecule and electron-substrate interactions. When the molecule is adsorbed at a solid surface the potential experienced by the probe electron may be represented as the sum of three terms: the electron-molecule potential, $V_M(\mathbf{r},\mathbf{R})$, the electron-substrate potential, $V_S(\mathbf{r})$, and an additional term, $\Delta V(\mathbf{r},\mathbf{R},\mathbf{R}_M)$, which describes both the distortion of the electron-surface potential by the molecule and the distortion of the electron-molecule potential by the surface molecule,

$$V(\mathbf{r},\mathbf{R},\mathbf{R}_M)=V_M(\mathbf{r},\mathbf{R},\mathbf{R}_M)+V_S(\mathbf{r})+\Delta V(\mathbf{r},\mathbf{R},\mathbf{R}_M). \tag{3}$$

If the electron-molecule interaction time is short compared with the time scale of any nuclear or center-of-mass motion of the molecule then, according to the Born-Oppenheimer approximation, $\Psi(\mathbf{r},\mathbf{R})$ can be separated into a product of the vibrational wave function of the target molecule, $\chi_\nu(\mathbf{R})$, the wave function of the probe electron, $\psi(\mathbf{r})$, and a wave function describing the vibrational and librational motion of the molecule against the substrate, $\zeta_\mu(\mathbf{R}_M)$,

$$\Psi(\mathbf{r},\mathbf{R})=\chi_\nu(\mathbf{R})\psi(\mathbf{r},\mathbf{R},\mathbf{R}_M)\zeta_\mu(\mathbf{R}_M). \tag{4}$$

This adiabatic approximation is assumed to hold in all of the calculations described in this paper, although the method can be generalized to include nuclear motion at additional computational cost. Consequently, in its present form, our approach is most appropriate for the description of electron-molecule scattering processes where substantial nuclear motion does not occur during the lifetime of the intermediate state. For the main focus of this work, the resonance lifetime for vibrational excitation via the formation of shape resonances ($\tau_R\approx1$ fs), the adoption of this approximation is not a serious limitation of the method. Further, for simplicity we assume that the motion of the molecule against the surface occurs on a time scale (≈100 fs) that is much longer than both the intramolecular vibrational motion (≈10 fs) and the resonance lifetime (≈1 fs). Consequently, we assume that $\mathbf{R}_M$ is fixed during the lifetime of the resonance. However, we note that the Born-Oppenheimer approximation may be inadequate for the description of dynamical events that are sensitive to those negative ions that survive for substantially longer than the mean lifetime τ_R. An example of such a process is resonance-assisted desorption, as has been pointed out by both Harris, Holloway, and Darling[17] and Gadzuk.[35]

B. The electron-molecule potential

We employ a scattered-wave $X\alpha$ (SW-$X\alpha$) description of the molecular potential, adopted by Davenport, Ho, and Schrieffer[36] from the original work of Dill and co-workers,[37,38] in which the molecular potential is partitioned into three regions as shown in Fig. 1. Inside each atomic sphere (region I) and beyond the outer sphere (region III), the potential is spherically averaged. Each atom (region I) can then be described by its scattering phase shifts. In the interstitial region (region II), the potential is volume averaged to a constant. Inside the outer molecular sphere, the exchange-correlation potential can be modeled by a local potential of $X\alpha$ form,

$$V_{\rm xc}(\mathbf{r})=-3\alpha\left(\frac{3n(\mathbf{r})}{8\pi}\right)^{1/3}, \tag{5}$$

where n is the electron density and α is an adjustable parameter of order $0.7\lesssim\alpha\lesssim1$. For the free molecule, the $X\alpha$ potential is matched onto the classical polarization potential,

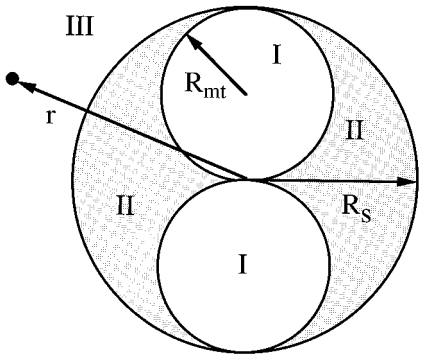

FIG. 1. A schematic illustration of the partitioning of the model electron-molecule interaction potential employed in the layer-KKR calculation for a homonuclear diatomic molecule. Each atomic sphere (region I) has a radius equal to the atomic muffin-tin radius (R_{mt}) and the potential inside is spherically averaged and can be described by a set of atomic phase shifts. In the interstitial region (region II), bounded by the outer-sphere radius, R_s and R_{mt}, the potential is volume averaged to a constant. Beyond the outer sphere (region III), the potential is a spherically averaged classical polarization potential (see text). r is the position vector of the probe electron.

$$V_{III}(\mathbf{r}) = -\frac{\alpha_0}{2r^4} + V_0 e^{-2r}, \tag{6}$$

at the outer molecular sphere. V_0 parametrizes the exponential cutoff of the $X\alpha$ potential, and is fitted by matching the interior and exterior potentials at the outer molecular sphere.

In more sophisticated R-matrix calculations for free molecules,[39,40] it is known that the calculated resonance energies and cross sections are sensitive to the truncation of the polarization potential at the outer sphere. Consequently, our approach is to parametrize the eigenphase shifts of the resonant channel and fit them to either the experimentally determined, or calculated, resonance energy and width of the free molecule (see Sec. II C). The eigenphase shifts of the nonresonant channels are computed by the standard SW-$X\alpha$ method.[36–38] For the $^2\Pi_g$ shape resonance in Ag(111)-N_2, we have demonstrated good agreement between this description of the molecular scattering and a coupled angular mode (CAM) calculation in which the long-range polarization potential is included explicitly.[41]

C. Multiple scattering representation of the probe electron

In an angular momentum representation, the probe electron wave function on the molecular sphere of the adsorbed molecule can be expanded as a set of spherical partial waves about the center of mass of the molecule. The (incoming) spherical wave field can be written as

$$\psi^-(\mathbf{r}) = \sum_{lm} A_{lm} j_l(\kappa r) Y_{lm}(\hat{\mathbf{r}}), \tag{7}$$

where κ is the electron wave vector. If the electron excites a vibrational transition $\nu \rightarrow \nu'$, then the outgoing wave field of the scattered electron is

$$\psi^+(\mathbf{r}) = \sum_{l'm'} \sum_{lm} (T^{\nu\nu'}_{l'm',lm} A_{lm}) h^{(1)}_{l'}(\kappa' r) Y_{l'm'}(\hat{\mathbf{r}}), \tag{8}$$

where κ' is the wave vector of the scattered electron,

$$\kappa' = \sqrt{\kappa^2 - (\nu' - \nu)\hbar\omega}, \tag{9}$$

and ω is the fundamental frequency of the molecular vibration excited by the electron scattering. In calculations of impact scattering in HREELS, it is commonly assumed that $\kappa' = \kappa$. This is a reasonable assumption when the incident electron energy is much greater than the vibrational level spacing ($\hbar\omega$), but is a poor approximation for low-energy resonances such as the $^2\Pi_g$ shape resonance in N_2 which lies at 2.3 eV. In this case, electrons which excite high-order intramolecular vibrations ($\hbar\omega \approx 0.28$ eV) detach very close to the threshold where the scattering properties of the substrate vary very rapidly with electron energy.[42] Consequently the assumption that $\kappa' = \kappa$ is not made in the calculation described in this paper.

In an angular momentum basis set, T describes the scattering of an electron from a partial wave (l,m) to a partial wave (l',m') by the adsorbed molecule which was initially in the vibrational state ν, but is left in the vibrational state ν'. T is obtained by integrating over the nuclear coordinates $\mathbf{R}$ corresponding to the two vibrational eigenstates

$$T^{\nu\nu'}_{l'm',lm} = \int\int\int \chi_\nu(\mathbf{R}) T_{l'm',lm}(\mathbf{R}) \chi_{\nu'}(\mathbf{R}) d\mathbf{R}, \tag{10}$$

where $T(\mathbf{R})$ indicates that the molecular scattering is computed for a fixed set of nuclear coordinates. T is the full scattering matrix of the adsorbed molecule and therefore describes the (multiple) scattering of the probe electron by the molecule surface system represented, at fixed $\mathbf{R}$ and $\mathbf{R}_M$, by the potential $V(\mathbf{r},\mathbf{R},\mathbf{R}_M)$ [see Eq. (3)].

When the molecule is far from the surface, $\Delta V \rightarrow 0$, and T is equal to the molecular scattering matrix M, which describes the (inelastic) scattering of (incoming) spherical waves by the free molecule,

$$j_l(\kappa r) Y_{lm}(\hat{\mathbf{r}}) \rightarrow j_l(\kappa r) Y_{lm}(\hat{\mathbf{r}}) + \sum_{l'm'} M^{\nu\nu'}_{l'm',lm} h^{(1)}_{l'}(\kappa r) \times Y_{l'm'}(\hat{r}). \tag{11}$$

The poles of M are the scattering resonances of the free molecule. M reflects the symmetry of the molecule. For example, for a diatomic molecule with its axis oriented parallel to the z axis, cylindrical symmetry demands that M is diagonal in m,

$$M_{lm,l'm'} = M_{ll'} \delta_{mm'}. \tag{12}$$

As usual, diagonalization of M yields the eigenphase shifts of the molecule.[40]

Using the model potential described in Sec. II B, the elements of M corresponding to the nonresonant channels are calculated using a standard SW-$X\alpha$ calculation.[38,37] The eigenphase shifts of the resonant channel(s) are fitted to R-matrix calculations[40] or fitted to the experimentally determined resonance energy and width. Thus it is assumed that M is transferable between the free and adsorbed molecule, an approximation that is justified in the limit where $\Delta V \rightarrow 0$.

Such an approximation is reasonable if it is assumed that the change in the surface potential due to the presence of the molecule may be neglected. This is a reasonable assumption for the main focus of this work which is resonance scattering by physisorbed molecules. The validity of this approximation has been discussed by Nordlander.[43] Further, in the present theory, a one-electron description is employed. This approximation is justified for the treatment of one-electron processes, such as resonance electron scattering by a molecular ion,[43] but cannot describe many-electron processes such as Auger deexcitation, which may be important when the molecule is very close to the surface.[16]

D. Electron scattering by the adsorbed molecule

To describe the electron scattering by the adsorbed molecule, we need to calculate how the scattering of the isolated (free) molecule is modified by the presence of the substrate. To do this we sum the multiple electron scattering paths between the molecule and the substrate. This summation is achieved by first representing the probe electron wave function in an angular momentum basis. Then the molecular scattering is described by M and the effect of the substrate and barrier scattering can be represented, quite generally, as a scattering matrix S that couples outgoing spherical waves originating from the molecule at the origin to incoming spherical waves centered upon the molecular center of mass,

$$h_l^{(1)}(\kappa r)Y_{lm}(\hat{\mathbf{r}}) \rightarrow h_l^{(1)}(\kappa r)Y_{lm}(\hat{\mathbf{r}}) + \sum_{l'm'} S_{l'm',lm} j_{l'}(\kappa r) Y_{l'm'}(\hat{\mathbf{r}}). \quad (13)$$

Here we consider only elastic electron scattering by the substrate so that $\kappa = \kappa'$.

The scattering of the probe electron by the substrate can be described in a plane-wave basis. Since the substrate possesses two-dimensional periodicity parallel to the surface, the substrate and each atomic plane within the substrate couple together only those plane waves whose parallel momentum differs by a two-dimensional (2D) reciprocal lattice vector $\mathbf{g}$. The parallel wave vector in the first surface Brillouin zone is labeled $\mathbf{k}_\parallel$. Using this notation, the probe electron scattering in the substrate can be obtained by computing the $\mathbf{k}_\parallel$-resolved reflection matrices of the left (L) and right

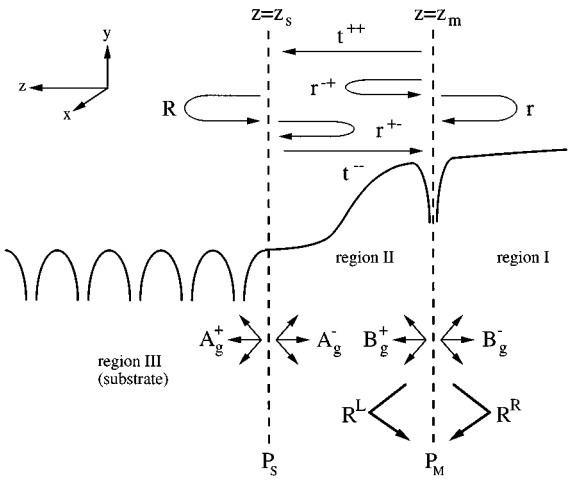

FIG. 2. A schematic illustration of the model electron-substrate interaction potential employed in the layer-KKR calculation. Regions I and II consist of an uncorrugated surface barrier, parametrized and fitted to the binding energy of image states. Region III contains the substrate which consists of a stack of atomic planes parallel to the surface. The substrate plane ($z=z_s$) lies one-half of an interplanar spacing outside the last atomic plane of the substrate. The molecular plane ($z=z_m$) cuts through the molecular center of mass. At $z=z_s$ and $z=z_m$, the electron wave function is expanded in a plane-wave basis.

(R) half spaces relative to a plane (P_M), parallel to the substrate, that passes through the molecular center of mass (the z axis is normal to the substrate and points *into* the substrate; see Fig. 2). At P_M, a plane wave with parallel momentum $\mathbf{k}_\parallel + \mathbf{g}$, initially traveling in the $+z$ direction, is reflected by the left half-space as follows:

$$e^{i(\mathbf{k}_\parallel+\mathbf{g})\cdot\mathbf{r}_\parallel} e^{+iK^+_{\mathbf{g}z}(z-z_m)} \rightarrow e^{i(\mathbf{k}_\parallel+\mathbf{g})\cdot\mathbf{r}_\parallel} e^{+iK^+_{\mathbf{g}z}(z-z_m)} + \sum_{\mathbf{g}'} R^L_{\mathbf{g}'\mathbf{g}} e^{i(\mathbf{k}_\parallel+\mathbf{g}')\cdot\mathbf{r}_\parallel} e^{iK^-_{\mathbf{g}'z}(z-z_m)} \quad (14)$$

where R^L is the reflection matrix of the left half-space, $\mathbf{g}$ is a reciprocal lattice vector of the substrate, and

$$K^\pm_{\mathbf{g}z} = \pm\sqrt{2[E-V(z_m)] - |\mathbf{k}_\parallel+\mathbf{g}|^2} \quad (15)$$

is the component of the electron wave vector normal to the substrate. The reflection matrix of the right half space, R^R, is defined in a similar fashion.

Once R^R and R^L have been determined from a multiple scattering calculation for the substrate (see Secs. II E and II F), S is obtained by projection from a plane wave to an angular momentum basis. For each $\mathbf{k}_\parallel$ component of the electron wave field,

$$\tau_{lm,l'm'}(\mathbf{k}_\parallel,E) = \sum_{\mathbf{g}}\sum_{\mathbf{g}'} \tilde{\Lambda}^+_{lm,\mathbf{g}}(\mathbf{k}_\parallel)[(1-R^RR^L)^{-1}R^R]_{\mathbf{g}\mathbf{g}'}\Lambda^-_{\mathbf{g}',l'm'}(\mathbf{k}_\parallel) + \tilde{\Lambda}^-_{lm,\mathbf{g}}(\mathbf{k}_\parallel)[R^L(1-R^RR^L)^{-1}]_{\mathbf{g}\mathbf{g}'}\Lambda^+_{\mathbf{g}',l'm'}(\mathbf{k}_\parallel) + \tilde{\Lambda}^-_{lm,\mathbf{g}}(\mathbf{k}_\parallel) \times [R_L(1-R^RR^L)^{-1}R^R]_{\mathbf{g}\mathbf{g}'}\Lambda^-_{\mathbf{g}',l'm'}(\mathbf{k}_\parallel) + \tilde{\Lambda}^+_{lm,\mathbf{g}}(\mathbf{k}_\parallel)[(1-R^RR^L)^{-1}R^RR^L]_{\mathbf{g}\mathbf{g}'}\Lambda^+_{\mathbf{g}',l'm'}(\mathbf{k}_\parallel). \quad (16)$$

The operator Λ projects outgoing spherical waves into a plane-wave basis,

$$\Lambda^{\pm}_{lm,\mathbf{g}}(\mathbf{k}_{\parallel}) = \frac{2\pi i}{\Delta\kappa|K_{\mathbf{g}z}|}\, Y_{lm}(\hat{\mathbf{K}}^{\pm}_{\mathbf{g}}), \tag{17}$$

where Δ is the area of the surface unit cell of the substrate. The inverse operator $\tilde{\Lambda}$ (Ref. 44) projects plane waves into an angular momentum basis,

$$\tilde{\Lambda}^{\pm}_{\mathbf{g},lm}(\mathbf{k}_{\parallel}) = 4\pi i^{l} Y^{*}_{lm}(\hat{\mathbf{K}}^{\pm}_{\mathbf{g}}). \tag{18}$$

The full scattering matrix of the surface is obtained by integration of τ over the two-dimensional Brillioun zone (area Ω) containing $\mathbf{k}_{\parallel}$ (see Sec. II H),

$$S_{lm,l'm'}(E) = \frac{1}{\Omega}\int\int_{\Omega} \tau_{lm,l'm'}(\mathbf{k}_{\parallel},E)\,\mathbf{d}^2\mathbf{k}_{\parallel}. \tag{19}$$

Having obtained M and S, the full scattering matrix of the molecule-surface system is obtained by summing the multiple scattering series,

$$T(E) = M + MSM + MSMSM + \cdots = M(1-SM)^{-1}. \tag{20}$$

Explicitly,

$$T_{l'm',lm}(E,\mathbf{R},\mathbf{R}_M) = [M(\mathbf{R})[1-S(\mathbf{R}_M)M(\mathbf{R})]^{-1}]_{l'm',lm}, \tag{21}$$

where M is evaluated for fixed nuclear coordinates and S is evaluated for a fixed position of the molecule relative to the substrate.

Our basic approach to the computation of the reflection matrices of the left and right half spaces, relative to P_M, is to partition the molecule-substrate potential into distinct regions where the multiple scattering problem can be solved separately. Then the probe electron scattering can be constructed by summing the multiple electron scattering pathways between these regions. Specifically, the interaction potential experienced by the probe electron is separated into three regions by two planes parallel to the surface (see Fig. 2). The first plane, P_M, was defined earlier and passes through the center of mass of the molecule at $z=z_m$. The second plane, P_S, is positioned a distance of one-half of the bulk interplanar spacing above the top layer of substrate atoms at $z=z_s$. The region $z\geqslant z_s$ contains the crystalline substrate that consists of a stack of atomic planes parallel to the surface. The region $z\leqslant z_s$ contains a superposition of the local molecular potential and the surface barrier potential that asymptotically matches onto the classical image potential for $z\to-\infty$.

At each matching plane, the probe electron wave function may be expressed as a sum over plane waves such that

$$\psi(\mathbf{r}) = \sum_{\mathbf{k}_{\parallel}}\sum_{\mathbf{g}} A^{+}_{\mathbf{g}}(\mathbf{k}_{\parallel}) e^{i(\mathbf{k}_{\parallel}+\mathbf{g})\cdot\mathbf{r}_{\parallel}} e^{iK^{+}_{\mathbf{g}z}(z-z_s)} + A^{-}_{\mathbf{g}}(\mathbf{k}_{\parallel}) e^{i(\mathbf{k}_{\parallel}+\mathbf{g})\cdot\mathbf{r}_{\parallel}} e^{iK^{-}_{\mathbf{g}z}(z-z_s)} \quad \text{at } P_S \tag{22}$$

and

$$\psi(\mathbf{r}) = \sum_{\mathbf{k}_{\parallel}}\sum_{\mathbf{g}} B^{+}_{\mathbf{g}}(\mathbf{k}_{\parallel}) e^{i(\mathbf{k}_{\parallel}+\mathbf{g})\cdot\mathbf{r}_{\parallel}} e^{iK^{+}_{\mathbf{g}z}(z-z_m)} + B^{-}_{\mathbf{g}}(\mathbf{k}_{\parallel}) e^{i(\mathbf{k}_{\parallel}+\mathbf{g})\cdot\mathbf{r}_{\parallel}} e^{iK^{-}_{\mathbf{g}z}(z-z_m)} \quad \text{at } P_M. \tag{23}$$

At P_S, the scattering by the substrate alone is described by the $\mathbf{k}_{\parallel}$-resolved reflection matrix of the substrate $R_{\mathbf{g}\mathbf{g}'}$ (not to be confused with the vector $\mathbf{R}$, defined earlier, that describes the internuclear coordinates). Then, in the absence of any scattering in the region $z\leqslant z_s$,

$$A^{-}_{\mathbf{g}}(\mathbf{k}_{\parallel}) = \sum_{\mathbf{g}'} R_{\mathbf{g}\mathbf{g}'}(\mathbf{k}_{\parallel}) A^{+}_{\mathbf{g}'}(\mathbf{k}_{\parallel}), \quad z=z_s. \tag{24}$$

As is described in Sec. II F, the reflection matrix $R_{\mathbf{g}\mathbf{g}'}$ is determined from a layer-KKR calculation for a stack of atomic planes that represent the bulk termination of the solid.

At P_M, the substrate scattering in the right half space is determined by the barrier potential that lies beyond the molecular plane. Then, in the absence of any scattering in the region $z\geqslant z_m$, the matching condition at P_M can be written in terms of a $\mathbf{k}_{\parallel}$-resolved barrier reflection matrix $r_{\mathbf{g}\mathbf{g}'}$ (not to be confused with the probe electron position vector $\mathbf{r}$, defined earlier),

$$B^{+}_{\mathbf{g}}(\mathbf{k}_{\parallel}) = \sum_{\mathbf{g}'} r_{\mathbf{g}\mathbf{g}'}(\mathbf{k}_{\parallel}) B^{-}_{\mathbf{g}'}(\mathbf{k}_{\parallel}), \quad z=z_m. \tag{25}$$

As is described in Sec. II E, the barrier reflection matrix $r_{\mathbf{g}\mathbf{g}'}$ is determined by numerical integration of the Schrödinger equation from $z=-\infty$ to $z=z_m$.

The plane-wave amplitudes at P_M ($A^{\pm}_{\mathbf{g}}$) and P_s ($B^{\pm}_{\mathbf{g}}$) are linked together by the transmission and reflection matrices of the barrier slice between this pair of planes, denoted r^{+-}, r^{-+}, t^{++}, and t^{--} (see Fig. 2). Then, in the absence of any scattering in the regions $z\geqslant z_s$ and $z\leqslant z_m$, the matching conditions across the barrier slice are

$$A^{+}_{\mathbf{g}}(\mathbf{k}_{\parallel}) = \sum_{\mathbf{g}'} t^{++}_{\mathbf{g}\mathbf{g}'}(\mathbf{k}_{\parallel}) B^{+}_{\mathbf{g}'}(\mathbf{k}_{\parallel}) + r^{+-}_{\mathbf{g}\mathbf{g}'}(\mathbf{k}_{\parallel}) A^{-}_{\mathbf{g}'}(\mathbf{k}_{\parallel}), \tag{26}$$

$$B^{-}_{\mathbf{g}}(\mathbf{k}_{\parallel}) = \sum_{\mathbf{g}'} t^{--}_{\mathbf{g}\mathbf{g}'}(\mathbf{k}_{\parallel}) A^{-}_{\mathbf{g}'}(\mathbf{k}_{\parallel}) + r^{-+}_{\mathbf{g}\mathbf{g}'}(\mathbf{k}_{\parallel}) B^{+}_{\mathbf{g}'}(\mathbf{k}_{\parallel}). \tag{27}$$

Finally, reflection matrices of the left and right half spaces, $R^{L}_{\mathbf{g}\mathbf{g}'}$, and $R^{R}_{\mathbf{g}\mathbf{g}'}$, respectively, are obtained by summing the multiple scattering paths between P_M and P_S,

$$\begin{aligned} \mathbf{R}^{R} &= \mathbf{r}, \\ \mathbf{R}^{L} &= \mathbf{r}^{+-} + \mathbf{t}^{--}(1-\mathbf{R}\mathbf{r}^{+-})^{-1}\mathbf{R}\mathbf{t}^{++}. \end{aligned} \tag{28}$$

Combination of Eqs. (28) and (16) permits the computation of the substrate scattering matrix S from the reflection matrix of the substrate $R_{\mathbf{g}\mathbf{g}'}$, the barrier reflection matrix $r_{\mathbf{g}\mathbf{g}'}$, and the reflection and transmission matrices of the barrier slice, $r^{+-}_{\mathbf{g}\mathbf{g}'}$, $r^{-+}_{\mathbf{g}\mathbf{g}'}$, $t^{++}_{\mathbf{g}\mathbf{g}'}$, and $t^{--}_{\mathbf{g}\mathbf{g}'}$. The computational methods used to calculate these six matrices are described in the next three sections.

E. Electron scattering by the surface barrier

The simplest approximation to the barrier scattering would be to neglect it completely, as is done in the standard theory of low-energy electron diffraction (LEED).[45] This approximation is adequate when the kinetic energy of the probe electron, i.e., $E>50$ eV, is large compared to the surface barrier height (the sum of the Fermi energy and the work function, $E_F+\phi\sim 10-15$ eV). Clearly, this approximation is inadequate for the description of resonance scattering by adsorbed molecules, where the electron energy is usually below 20 eV and often only a few electronvolts above the vacuum level. Consequently, for resonance scattering, the barrier potential must be included explicitly.

The electron scattering by the substrate barrier potential for $z\leqslant z_s$ is obtained by numerically integrating the Schrödinger equation through the barrier region. In general, the barrier potential is corrugated with a 2D periodicity commensurate with that of the substrate (in the case of an isolated adsorbed molecule) or that of the molecular overlayer (for an ordered overlayer of molecules). However, in all applications to date, we have employed an uncorrugated surface barrier potential $V_b(\mathbf{r})=V_b(z)$. $V_b(z)$ is obtained by fitting a parametrized surface barrier shape to the binding energy of image states, and gives an adequate description of electron scattering in very low-energy electron diffraction (VLEED) (Refs. 46 and 47) for which the electron energies are comparable to those considered here. In the absence of further *a priori* information about the other Fourier components of the barrier potential, the introduction of corrugation into the model potential would simply increase the number of free parameters in the calculation. Consequently, corrugation is neglected in the present implementation of the LKKR method, although it could be easily incorporated into the computational method.

For a given $\mathbf{k}_\parallel$, the probe electron wave function in the barrier region may be written as a Fourier expansion over the 2D reciprocal lattice vectors of the substrate $\mathbf{g}$,

$$\psi(\mathbf{k}_\parallel,\mathbf{r})=\sum_{\mathbf{g}}\ \psi_{\mathbf{g}}(z)e^{i(\mathbf{k}_\parallel+\mathbf{g})\cdot\mathbf{r}_\parallel}. \tag{29}$$

In atomic units, the Schrödinger equation satisfied by the wave function is

$$-\frac{1}{2}\frac{d^2\psi_{\mathbf{g}}(z)}{dz^2}+V_b(z)\psi_{\mathbf{g}}(z)=E_\perp\psi_{\mathbf{g}}(z), \tag{30}$$

where $E_\perp$ is the ''normal'' component of the electron energy,

$$E_\perp=E-\tfrac{1}{2}|\mathbf{k}_\parallel+\mathbf{g}|^2. \tag{31}$$

For each $\mathbf{k}_\parallel$ and $\mathbf{g}$, a four-point Runge-Kutta algorithm is used to numerically integrate Eq. (30) between z_m and a plane far away from the crystal, $z_{-\infty}$, and between z_m and the substrate plane, z_s. The logarithmic derivative of $\psi_{\mathbf{g}}(z)$ at the matching planes allows the calculation of the reflection and transmission matrices r^{+-}, r^{-+}, t^{++}, and t^{--} (see Fig. 2). For example, if numerical integration of Eq. (30) from $z_{+\infty}\rightarrow z_m$ results in values of $\psi_{\mathbf{g}}(z=z_m)$ and $\psi'_{\mathbf{g}}(z=z_m)$, respectively, for the electron wave function and its derivative (with respect to z) at $z=z_m$, then the barrier reflection matrix is

$$r_{\mathbf{g}\mathbf{g}'}(\mathbf{k}_\parallel)=\frac{iK^+_{\mathbf{g}z}\psi_{\mathbf{g}}(z_m)+\psi'_{\mathbf{g}}(z_m)}{iK^+_{\mathbf{g}z}\psi_{\mathbf{g}}(z_m)-\psi'_{\mathbf{g}}(z_m)}\,e^{2iK^+_{\mathbf{g}z}z_m}\delta_{\mathbf{g}\mathbf{g}'}. \tag{32}$$

In the present work, the barrier potential is parametrized according to the model proposed by Jennings and co-workers,[48,46]

$$V(z)=\frac{1}{2(z-z_0)}\{1-\exp[\lambda(z-z_0)]\},\quad z\leqslant z_0 \tag{33}$$

and

$$V(z)=\frac{-U_0}{\alpha\,\exp[-\beta(z-z_0)]+1},\quad z\geqslant z_0 \tag{34}$$

where α and β are constants determined by matching $V(z)$ at z_0 ($\beta=U_0/A$, $\alpha=2U_0/\lambda-1$). Inside the substrate, as $z\rightarrow+\infty$, the potential approaches a constant value of U_0, which is the inner potential of the substrate. This model has an asymptotic form, $z\rightarrow-\infty$, similar to a shifted image potential, where z_0 is the effective image plane location. λ is a measure of the ''saturation'' of the barrier; for many metal surfaces $\lambda\approx 2U_0$. This model potential has a similar shape to the calculated effective potential for a jellium surface and reproduces very closely the effective barrier potential obtained from density-functional calculations of transition-metal surfaces such as W(100).[48]

For many single-crystal substrates the values of U_0, λ, and z_0 (relative to the first atomic plane) have been determined from the binding energy of image states.[49] We note that in the LKKR calculation the barrier potential must be matched to the constant interstitial potential at the substrate plane P_s, $z=z_s$. This is done by setting the muffin tin zero for the substrate atoms equal to the value of $V(z=z_s)$ from Eqs. (33) and (34).

F. Calculation of the reflection matrix of the substrate

The substrate reflection matrix $R_{\mathbf{g}\mathbf{g}'}$ [Eq. (24)] describes the reflection of plane waves defined with an origin in the substrate plane P_s (see Fig. 2). With minor modifications, the computational approach used to evaluate $R_{\mathbf{g}\mathbf{g}'}$ is closely related to the methods employed in LEED theory to evaluate *IV* spectra from single-crystal substrates.[45] These methods have also been used as the foundation of a layer-KKR approach to the calculation of bulk and interface properties, developed more recently by Maclaren, Crampin, and Vvedensky.[44]

The substrate is modeled as a stack of monatomic planes parallel to the surface and, consistent with other layer-KKR-based theories,[44,45] the atomic potentials of the substrate are of muffin-tin form with the interstitial potential volume averaged to a constant. The atomic phase shifts for the substrate atoms are determined from a self-consistent bulk layer-KKR calculation[44] starting from the free atomic potentials.

For a substrate with a single atom in the surface unit cell, the reflection and transmission matrices of a single atomic layer, $Q^{\pm\pm}$, may be expressed as

$$Q^{\pm\pm}_{\mathbf{gg}'}(\mathbf{k}_\parallel) = -\sum_{lm}\sum_{l'm'} \Lambda^{\pm}_{\mathbf{g},l'm'}(\mathbf{k}_\parallel) q_{lm,l'm'}(\mathbf{k}_\parallel) \tilde{\Lambda}^{\pm}_{\mathbf{g}',l'm'}(\mathbf{k}_\parallel), \tag{35}$$

where the projection operators $\Lambda^{\pm}$ and $\tilde{\Lambda}^{\pm}$ were defined earlier [Eqs. (17) and (18)] and

$$q_{lm,l'm'} = [(1-tG)^{-1}t]_{lm,l'm'}. \tag{36}$$

G is the lattice Green's function which may be expressed in terms of a real-space sum over the position vectors of all atoms within the layer $\mathbf{x}_j$,

$$G_{lm,l'm'}(\mathbf{k}_\parallel) = -8\pi i\kappa \sum_{l''m''}\sum_{j} i^{l''} C_{lm,l'm',l''m''} h^{(1)}_{l''}(\kappa x_j) \times Y_{l''m''}(_j) e^{i\mathbf{k}_\parallel\cdot\mathbf{x}_j}, \tag{37}$$

where $C_{lm,l'm',l''m''}$ is a Gaunt coefficient,

$$C_{lm,l'm',l''m''} = \int\int\int Y^*_{lm}(\hat{\mathbf{x}}) Y_{l'm'}(\hat{\mathbf{x}}) Y^*_{l''m''}(\hat{\mathbf{x}}) d\Omega_x. \tag{38}$$

The complete derivation leading to Eqs. (35) through (37) may be found in the book by Pendry.[45] The scattering paths within one atomic layer were summed in reciprocal space using the procedure described by Kambe[50–52] to generate G [Eq. (37)].

The atomic planes are assembled into the semi-infinite termination of the crystal surface using the layer-doubling algorithm[45] to sum the interlayer multiple scattering paths. The layer-doubling algorithm is based upon the formula for combining two atomic planes into a single scattering unit, described by reflection and transmission matrices for the paired layer $Q^{\pm\pm}_2$. Symbolically,

$$\begin{aligned} Q^{++}_2 &= Q^{++}(1-Q^{+-}Q^{-+})^{-1}Q^{++}, \\ Q^{--}_2 &= Q^{--}(1-Q^{-+}Q^{+-})^{-1}Q^{--}, \\ Q^{-+}_2 &= Q^{-+} + Q^{--}Q^{-+}(1-Q^{+-}Q^{-+})^{-1}Q^{++}, \\ Q^{+-}_2 &= Q^{+-} + Q^{++}Q^{+-}(1-Q^{-+}Q^{+-})^{-1}Q^{--}. \end{aligned} \tag{39}$$

Equation (39) is applied recursively to successively double the number of atomic layers in the stack, $n=2,4,8,16,\ldots$. Upon convergence, the reflection matrix of the substrate is obtained, $R=Q^{+-}_{n\to\infty}$. The rate of convergence of the layer-doubling algorithm is a function of the mean-free path of the electron in the substrate which, in the present calculation, is modeled by an imaginary component of the electron energy, V_{0i}.

As an illustration of the rate of convergence of the layer-doubling algorithm, and its dependence on the imaginary part of the electron energy, we display in Fig. 3 the relative error in the calculated reflectivity of Ag(111) for normal incidence [$R_{00}(\mathbf{k}_\parallel=0)$, $E=7$ eV], plotted as a function of the number of layer doublings. It is apparent that, in all of the cases considered, the layer-doubling algorithm rapidly converges until within five doublings (i.e., a slab of $2^5=32$ atomic layers) the relative error is smaller than 10^{-6}. Note that the reflectivity converges more rapidly as V_{0i} is increased and the electron penetration into the substrate is reduced. This behavior is typical of the convergence of the reflection matrix which is achieved for a stack of between 16 to 32 atomic planes that represent the termination of the crystal. Typically, the smallest value of V_{oi} employed in the calculation is 0.25 eV, which corresponds to a mean-free path of approximately 20 Å for a (real) electron energy of 2 eV and approximately 50 Å for an electron energy of 10 eV. Given that the interlayer spacing for Ag(111), $d=2.36$ Å, convergence of the reflection matrix is expected for a stack of between 8 and 20 atomic planes, in agreement with the empirical results presented in Fig. 3.

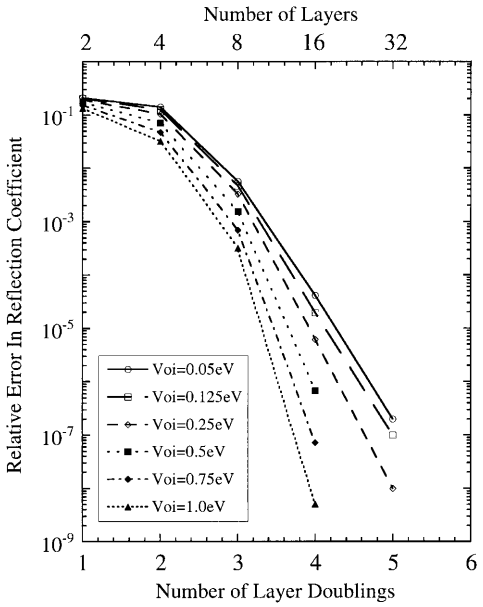

FIG. 3. The relative error in the calculated reflectivity of a Ag(111) substrate for normal incidence electrons with an energy of 7 eV [$|R_{00}(\mathbf{k}_\parallel)=0|^2$]. The error is plotted as a function of the number of layer doublings and the magnitude of the imaginary part of the electron energy V_{0i}. The relative error is defined as the fractional difference between the modulus of the reflectivity for a given number of layer doublings (N) and the value obtained for $N=7$ (128 layers). Note that the reflectivity converges more rapidly as V_{0i} is increased and the electron penetration into the substrate is reduced.

G. Location of the resonance poles: The resonance lifetime and energy

Having constructed a computational procedure which enables the calculation of $T(E)$, it remains to establish a method for locating the resonance poles of the adsorbed molecule. Formally, the resonance poles for scattering by the adsorbed molecule occur at complex energies in the lower half of the complex E plane,

$$E = E_r - i\frac{\Gamma}{2}. \tag{40}$$

The poles of $T(E)$ cannot be located directly by, for example, computing T for complex E and then performing a numerical search for the poles. Such a procedure would require the calculation of the substrate and molecular scattering matrices in the lower half of the complex E plane where the negative imaginary part of the energy would cause the

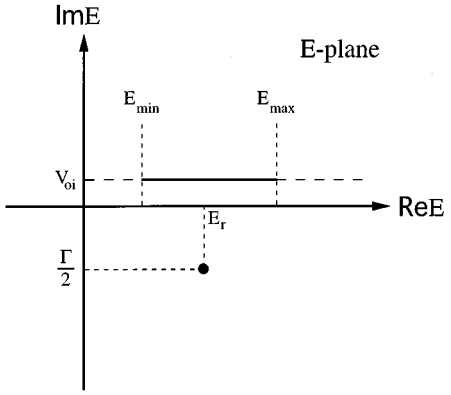

FIG. 4. A schematic diagram the scattering T matrix $T(E)$ in the complex-E plane. The LKKR calculation is performed slightly off the real axis in the upper half plane where the positive imaginary part of the electron energy ensures convergence of the multiple scattering summations. The poles of $T(E)$, corresponding to the resonances of the adsorbed molecule, are located in the lower half plane.

divergence of the layer-doubling algorithm used to compute S. In fact, the surface scattering matrix $S(E)$ can only be evaluated numerically for energies in the upper half plane where a small *positive* imaginary part of the energy damps the electron wave function and ensures convergence of numerical summation over multiple scattering paths within the substrate (see Fig. 4).

A practical method for determining the width and energy of an isolated resonance is to compute $T(E)$ for a range of electron energies along the real axis that includes E_r. Close to the resonance, one expects to find a peak in $|T(E)|$ at E_r. The lifetime, or scattering time delay, can be extracted from the variation of the resonant eigenphase shift evaluated at the resonance energy,[28]

$$\tau = \frac{1}{2}\frac{d\delta}{dE}. \tag{41}$$

This is essentially the procedure adopted by Teillet-Billy, Djamo, and Gauyacq within the context of the calculation of resonance properties by the CAM method.[28]

In the present case, this procedure must be modified because $S(E)$ can only be computed slightly off the real axis. We introduce a positive imaginary part to the potential, V_{0i}, and compute $S(E)$ for a range of electron energies just off the real axis, $S(E+iV_{0i})$, $E_{\min} \leqslant E \leqslant E_{\max}$ (see Fig. 4). To obtain $S(E)$ on the real axis we use numerical extrapolation: the substrate calculation is repeated for decreasing values of V_{0i} and polynomial extrapolation is used to estimate the limit as $V_{0i} \to 0$. For all substrates we have examined to date, quadratic extrapolation of $S(E)$ onto the real axis was found to be adequate.

As an illustration of this procedure, Fig. 5 shows the real and imaginary parts of $S_{10,10}(E+iV_{oi})$, plotted as a function V_{oi} for a point 3 Å above the top site of a Ag(111) substrate. Also shown is the variation of $S_{10,10}(E)$ on the real-E axis which was numerically determined by computing $S(E)$ for three values of the imaginary part of the electron energy, $V_{0i}^a = 0.25$ eV, $V_{0i}^b = 0.50$ eV, and $V_{0i}^c = 1.00$ eV and then using quadratic extrapolation to $V_{0i} = 0$,

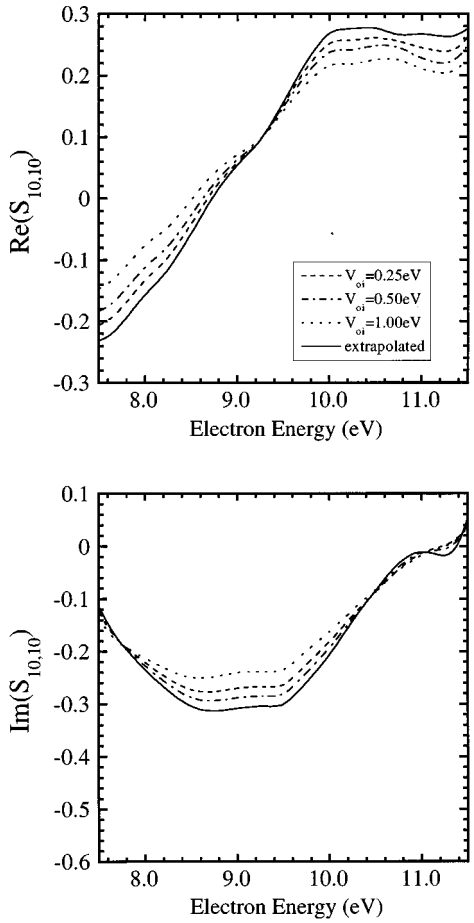

FIG. 5. The real and imaginary parts of $S_{10,10}(E+iV_{0i})$, calculated as a function V_{0i} for a point 3 Å above the top site of a Ag(111) substrate. The variation of $S_{10,10}(E)$ on the real-E axis (solid curve) was determined by extrapolation to $V_{0i}=0$ from $S(E+iV_{0i})$ computed for three values of the imaginary part of the electron energy: $V_{0i}=0.25$ eV (dashed curve), 0.50 eV (dot-dashed curve), and 1.00 eV (dotted curve).

$$S(E) \approx \tfrac{1}{6}[16S(E+V_{0i}^a) - 12S(E+V_{0i}^b) + 2S(E+V_{0i}^c)]. \tag{42}$$

For $V_{0i} < 0.25$ eV, the layer-doubling algorithm does not converge for the Ag(111) substrate.

From Fig. 5 it is apparent that the extrapolation procedure provides a reasonably convergent and stable approach to the computation of S on the real axis. We note that the magnitude of this element of the surface scattering matrix increases as V_{0i} is reduced. This is expected because a finite value of V_{0i} damps the electron wave field in the surface and reduces the overall reflectivity of the substrate.

An alternative procedure for locating the resonance energy and lifetime is based upon the method employed by Gerber and Herzenberg.[26] From Eq. (20), it is apparent that the problem of locating the resonance poles is equivalent to determining the complex energy roots of the secular equation,

$$|1 - S(E)M(E)| = 0. \tag{43}$$

The roots of Eq. (43) are obtained by analytic continuation of S and M into the lower half of the complex-E plane. We

proceed by fitting the determinant of Eq. (43), evaluated on the real-E axis, to a polynomial from which the roots may be obtained directly. Polynomial fitting is a numerically ill-conditioned problem. Therefore, it was necessary to exercise considerable numerical care in this part of the calculation. The polynomial fitting was performed in the least-squares sense using singular value decomposition to determine the coefficients of the lowest-order polynomial that adequately fitted the energy variation of the determinant. Using this procedure, the location of the resonance poles was stabilized for the majority of the applications we have considered to date.

Finally, we note that the simplest procedure for obtaining an estimate of the resonance energy and width is to least-squares fit $|T(E)|^2$ for the adsorbed molecule to a Breit-Wigner form,

$$|T(E)|^2 \propto \frac{(\Gamma/2)^2}{(E-E_r)^2+(\Gamma/2)^2}. \tag{44}$$

While this procedure has the virtue of being numerically simple and, more importantly, stable, it cannot correctly treat cases where the resonance profile of the adsorbed molecule is highly asymmetric, or when the resonance profile of the free molecule is not that of the prototypical single-channel resonance. Consequently, we employ this method only as a ''cross check'' of the resonance energy and width obtained using the two approaches described previously. Substantial differences between the results of this fitting procedure and the root-finding algorithm described above signal an instability in the fit of the determinant of Eq. (43) to a polynomial. In this case, the order of the polynomial used to fit the determinant must be either increased or decreased.

In Fig. 6 we illustrate the relative accuracy of these three approaches to the extraction of the resonance energy and width from the calculated energy dependence of the full scattering matrix $T(E)$. Figure 6 shows the resonance energy and width of the $^4\Sigma_u^-$ shape resonance of O_2 located above the top site of Ag(111), plotted as a function of the adsorption height. The resonance energy and width were determined by computing $T(E)$ on the real-E axis for $-1.5 \leqslant (E-E_r) \leqslant +1.5$ eV (E_r=9.5 eV for free O_2). The energy grid spacing was 0.1 eV so that $T(E)$ was computed for a total of 33 energy points. Shown in Fig. 6 are E_r and Γ calculated from (a) the time-delay matrix (dashed curve), (b) the roots of the secular equation [Eq. (43)] (solid curve), and (c) by fitting the resonance profile ($|T(E)|^2$) to a Breit-Wigner form (dotted curve).

From Fig. 6, it is apparent that the resonance energies and widths determined from the time-delay matrix and the roots of the secular equation agree within $\approx \pm 0.1$ eV. This represents a difference of less than $\approx \pm 2\%$ in the computed lifetime relative to that of the free molecule (Γ=3.4 eV). Fitting the resonance profile to a pure Breit-Wigner form (dotted curve) yields resonance energies and widths that are less accurate than the other two methods, because the profile of the adsorbed molecule is slightly asymmetric. Nevertheless, the error in the determined values of E_r and Γ is smaller than $\approx \pm 0.2$ eV.

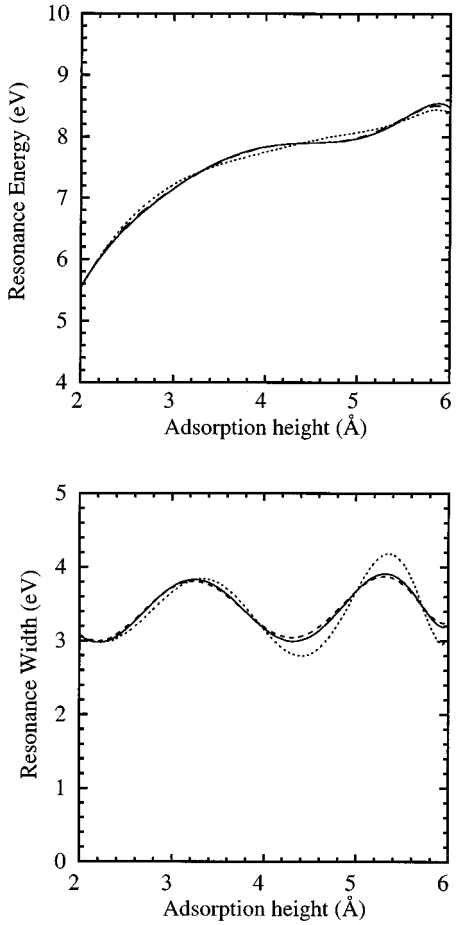

FIG. 6. The resonance energy and width of the $^4\Sigma_u^-$ shape resonance of O_2 located above the top site of Ag(111), plotted as a function of the molecular adsorption height. The resonance energy and width were determined from $T(E)$ using the three methods discussed in the text: Solid curve, from the roots of the secular equation [Eq. (43)]; dashed curve, the energy dependence of the resonant eigenphase shift; dotted curve, by least-squares fitting of ($|T(E)|^2$) to a Breit-Wigner form.

H. The Brillouin-zone integral

Having determined the $\mathbf{k}_\parallel$-resolved reflection and transmission matrices of the left and right half spaces relative to the molecular plane P_M, S is obtained by projection from a plane-wave to an angular momentum basis [Eq. (16)], followed by integration of τ over the two-dimensional Brillouin zone (area Ω) containing $\mathbf{k}_\parallel$ [Eq. (19)].

The integral over the Brillouin zone is performed by quadrature using the method of ''special points''[53] to sample the irreducible wedge of the surface Brillouin zone. In Fig. 7 we display the real and imaginary parts of one calculated element of S, $S_{10,10}(E)$, computed as a function of the number of special points (N) included in the irreducible wedge of the Brillouin zone. S was evaluated at a point 3 Å above the top site of a Ag(111) substrate for V_{0i}=0.25 eV. Clearly, for this substrate, a reasonable representation of S is obtained for N=45, while N=135 gives results which are almost indistinguishable from N=400.

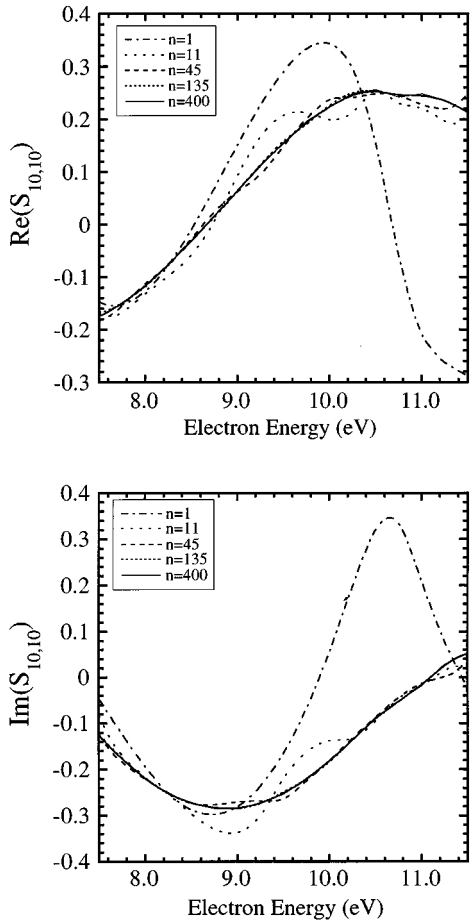

FIG. 7. The real and imaginary parts of one calculated element of the substrate scattering matrix, $S_{10,10}(E)$, computed at a point 3 Å above the top site of a Ag(111) substrate. The value of $S_{10,10}(E)$, as a function of the probe electron energy, is shown as a function of the number of special points (N) included in the irreducible wedge of the Brillouin-zone integral, $N=1$, 11, 45, 135, and 400. Note the close correspondence between S computed for $N=135$ and 400, indicating that $N=135$ special points are adequate for a convergent description of the substrate scattering matrix S.

III. THE NATURE OF THE SURFACE SCATTERING MATRIX

In this section, we discuss the general features of the calculated surface scattering matrix S, and how these features are related qualitatively to the variation of the resonance lifetime as a function of the adsorption height, site, and resonance energy. We consider resonance scattering from O_2 and N_2 physisorbed on Ag(111). Although S is independent of the identity of the adsorbate (since S describes only the probe electron scattering by the substrate), the symmetry of the molecular resonance determines which elements of S are important in changing the resonance behavior of a particular adsorbed molecule. The $^2\Pi_g$ (2.3 eV) shape resonance of free N_2 decays via the $d\pi$ partial wave. Consequently, when the molecule is adsorbed perpendicular to a surface, the coupling by the substrate between the $d\pi$ partial waves and between the $d\pi$ and $p\pi$ partial waves is particularly important.[26] The $^4\Sigma_u^-$ (9.5 eV) shape resonance of free O_2 decays via the $p\sigma$ partial wave. Therefore, when O_2 is adsorbed perpendicular to a surface, the coupling by the substrate between the $p\sigma$ partial waves and between the $p\sigma$ and s partial waves is particularly important.[26]

In Figs. 8 and 9, two elements of S, computed at a point 3.0 Å above the top [8(a) and 9(a)] and fcc-hollow [8(b) and 9(b)] sites of Ag(111) are displayed as a function of the probe electron energy. The elements of S correspond to the reflection of (outgoing) $p\sigma$ and $d\pi$ partial waves into an incoming wave of the same symmetry. These elements are relevant to the modification of the lifetime and energy of molecular resonances that decay predominantly via the $p\sigma$ and $d\pi$ partial waves: the $^4\Sigma_u^-$ shape resonance of O_2 which is formed at 9.5 eV in the gas phase and the $^2\Pi_g$ shape resonance of N_2 at 2.3 eV. These elements of S are plotted as a function of the electron energy relative to the vacuum level ($E_{\rm vac}=0$) and are computed with and without the inclusion of multiple electron scattering by the substrate. Specifically, the solid curves in Figs. 8 and 9 display S computed using the full LKKR calculation, while the dashed curves were computed by neglecting multiple scattering by the substrate. The latter calculation corresponds to an empty crystal approximation, where the substrate reflection matrix $R=0$ and the only substrate scattering is due to the barrier potential. Consequently, the empty-crystal results are directly comparable to calculations performed using the CAM method, where only the image screening of the probe electron by the substrate is considered.

Although the variation of the substrate scattering matrix elements as a function of the probe electron energy seems complex, some general trends may be extracted from Figs. 8 and 9. First we consider the matrix elements calculated including only the barrier scattering (i.e., the empty-crystal calculation) shown as the dashed curves in Figs. 8 and 9. Within the empty-crystal approximation, the S matrices computed for the distinct adsorption sites are identical since the crystalline substrate is not included in the calculation. From Figs. 8 and 9 we see that the S-matrix elements for the empty-crystal calculation display a rather simple structure as the probe electron energy is varied. As the electron energy is reduced, the magnitude of the matrix elements increases monotonically. This behavior follows from the energy dependence of reflectivity of the barrier, which is represented as a smooth step potential in the calculation. As the electron energy drops relative to the vacuum level, the reflectivity of the barrier increases and, consequently, the coupling between the incoming and outgoing partial waves centered on the molecule is enhanced.

By comparison, the calculated matrix elements including substrate scattering (i.e., by the full LKKR calculation, solid curves) exhibit qualitatively different behavior as the probe electron energy is increased above approximately 2 eV. For low electron energies, $E\lesssim 2$ eV, the S-matrix elements computed by the full LKKR calculation are quite similar to those computed without the inclusion of substrate scattering. Further, in this energy region, the S-matrix elements calculated for the top and fcc-hollow sites are similar, even though the substrate scattering is fully incorporated. The similarity of the matrix elements calculated with and without the inclusion of substrate scattering and for different adsorption sites suggests that the electron scattering by the barrier (i.e., the electrostatic screening of the negative ion) dominates the be-

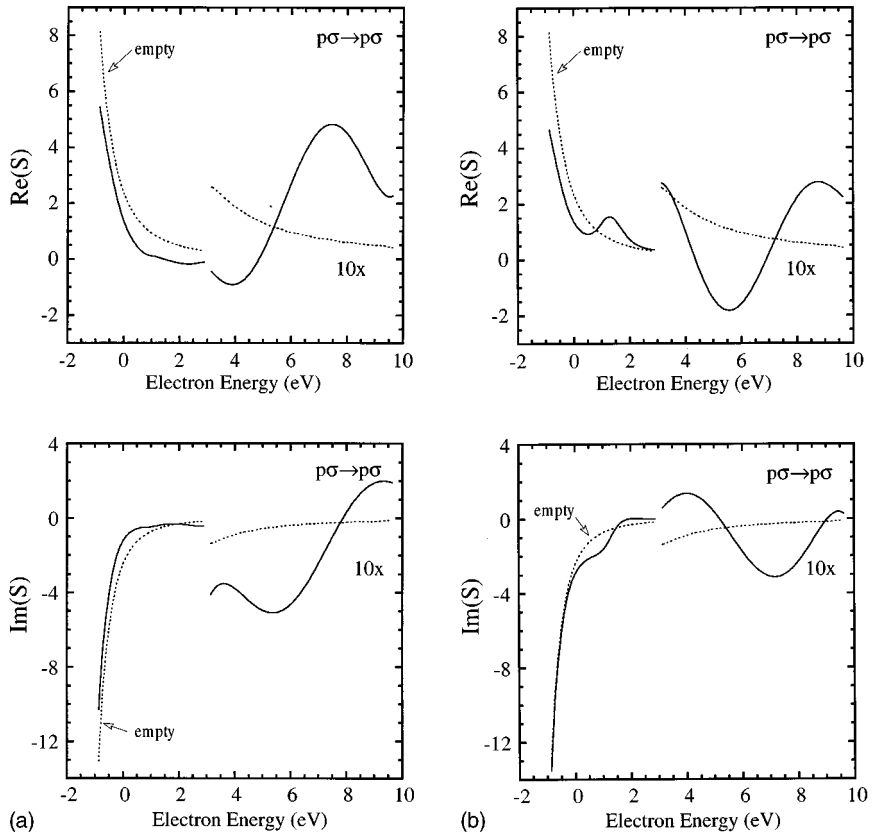

FIG. 8. The calculated S-matrix element ($S_{10,10}$) for $p\sigma \rightarrow p\sigma$ scattering for a point 3.0 Å above the top (a) and fcc-hollow (b) sites of Ag(111). The real and imaginary parts of S are plotted as a function of the electron energy, relative to the vacuum level of the substrate. Solid curve: full LKKR calculation that incorporates the electron scattering by the substrate. Dashed curve: empty-crystal calculation that includes scattering by the surface barrier only; electron scattering by the substrate is neglected.

havior of the S matrix, and consequently the resonance lifetime, for $E \lesssim 2$ eV. This behavior can be easily understood physically: When the electron energy is small compared to the barrier height [for Ag(111), 14.2 eV], the reflectivity of the surface barrier is close to unity. Consequently, as the electron energy approaches the vacuum level, the barrier dominates the reflection of the probe electron by the surface, provided the reflectivity of the substrate (represented by $R_{gg'}$) is significantly smaller than unity. This latter condition will be satisfied provided the electron energy does not lie within a projected band gap of the unoccupied electronic band structure of the crystalline substrate.

As the probe electron energy is increased, the barrier component of the substrate reflectivity drops. This effect can be seen in the empty-crystal calculations shown in Figs. 8 and 9 where the magnitude of the real and imaginary parts of S decrease monotonically with increasing energy. By contrast, the S-matrix elements computed using the full LKKR calculation develop distinct oscillatory structure when $E \gtrsim 2$ eV and do not decrease in magnitude as E increases. In this energy regime the S-matrix elements are determined predominantly by the interaction of the probe electron with the unoccupied electronic structure of the substrate because the barrier reflectivity is relatively small.

Finally, we display in Figs. 10 and 11 the behavior of the S-matrix elements, the resonance lifetime and energy for resonance scattering via the $^2\Pi_g$ (2.3 eV) state of N_2, and the $^4\Sigma_u^-$ (9.5 eV) state of O_2 physisorbed perpendicular to the top site of Ag(111). These quantities are plotted as a function of the adsorption height of the molecule, which is defined as the distance between the molecular center of mass and the center of the top plane of substrate atoms. As the adsorption height of the molecules is reduced, the calculated resonance energy falls towards the vacuum level; see the lower panels of Figs. 10 and 11.

First we consider resonance scattering via the $^2\Pi_g$ (2.3 eV) state of N_2, Fig. 10. In the gas phase, the resonance energy is 2.3 eV and drops to -1 eV below the vacuum level for an adsorption height of 2 Å. The upper panel of Fig. 10 shows the real and imaginary parts of the S-matrix element that couples together the $d\pi$ partial waves calculated within the empty-crystal approximation (dashed line) and for the full LKKR calculation (solid line). As the adsorption height is reduced, the magnitude of the S matrix element increases. Further, the S matrix elements computed using the full LKKR and empty-crystal calculations show similar behavior. This behavior is consistent with the earlier discussion of the energy dependence of the S-matrix elements: As the molecule approaches the surface the resonance energy drops from 2.3 eV towards the vacuum level. Thus, we are always in the low-energy regime where the S matrix is determined predominantly by the reflectivity of the barrier, which increases in magnitude as the adsorption height, and therefore the resonance energy, is reduced.

Qualitatively different behavior is observed for resonance scattering by the $^4\Sigma_u^-$ (9.5 eV) state of O_2 on the same sub-

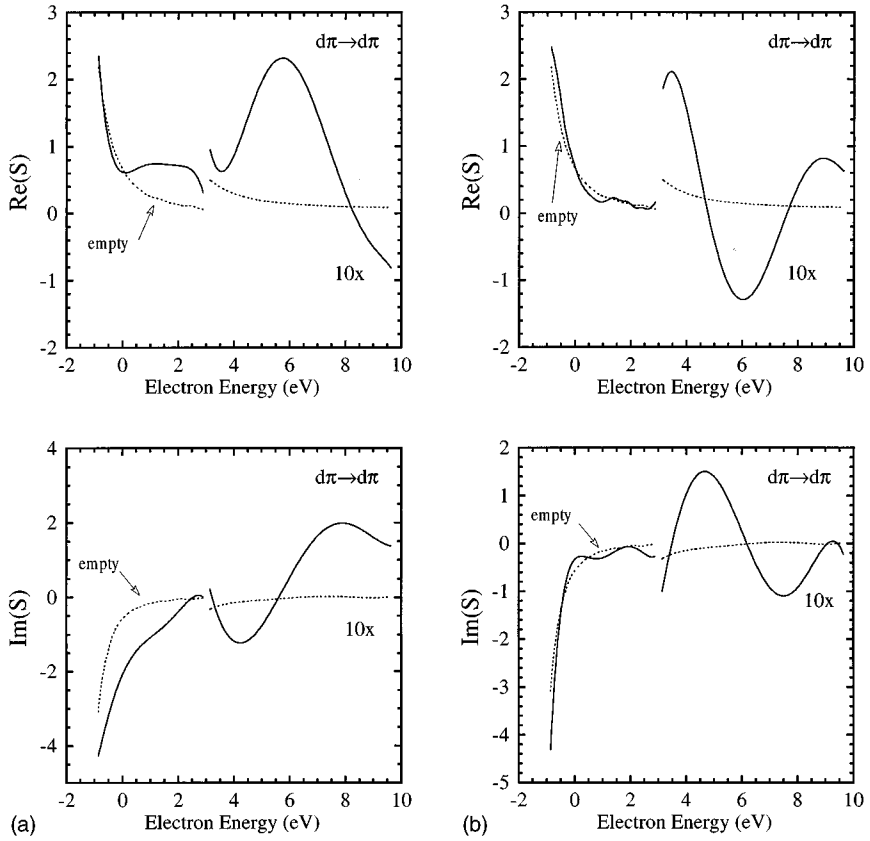

FIG. 9. As Fig. 8, for the calculated S matrix for $d\pi \rightarrow d\pi$ scattering.

strate, Fig. 11. When the molecule is far from the surface, the resonance lies in the range of energies where the substrate scattering matrix is an oscillatory function of energy (see Fig. 8). Thus, as the molecule approaches the surface, the resonance energy drops as a result of the image interaction and the lifetime oscillates. Only when the molecule is moved sufficiently close to the surface that the resonance energy, relative to the vacuum level, drops below approximately 2 eV is a monotonic decrease in the lifetime observed. In this case, the image interaction lowers the resonance energy to a value where the barrier reflectivity dominates the resonance behavior.

Finally, we note that it is possible to establish a qualitative link between the variation of the resonance lifetime and the S-matrix element corresponding to the resonant channel.[31,30] Consider a prototypical Breit-Wigner resonance in a single angular momentum channel (l,m). Then the corresponding element of M behaves as

$$M_{lm,lm} \equiv M = \frac{-i\Gamma}{2(E-E_r)+i\Gamma}. \tag{45}$$

Compared to the free molecule, the substrate alters the electron scattering states by partially reflecting outgoing spherical waves back towards the molecule. Thus, for the adsorbed molecule, the matrix element corresponding to the resonant channel becomes

$$M \rightarrow M' = M + MSM + MSMSM + \cdots = M(1-SM)^{-1}, \tag{46}$$

where $S = S_{lm,lm}$. If it is assumed that the energy variation of the molecular scattering amplitude occurs much more rapidly than for $S(E)$ (i.e., the molecular resonance occurs well away from any substrate resonances), then $S(E)$ can be replaced with its value on resonance, $S = S(E_r)$, and

$$M' \approx \frac{-i\Gamma}{2\left[E - \left(E_r + \frac{\Gamma}{2}\,\mathrm{Im}\,S\right)\right] + i\Gamma(1+\mathrm{Re}\,S)}. \tag{47}$$

Comparing Eqs. (47) and (45) we see that the effect of the substrate scattering is to shift the poles of the scattering amplitude, so that the resonance energy and width of the adsorbed molecule become

$$E_r \rightarrow E_r\left(1 + \frac{\Gamma}{2E_r}\,\mathrm{Im}\,S\right), \tag{48}$$

$$\Gamma \rightarrow \Gamma(1+\mathrm{Re}\,S). \tag{49}$$

Consequently, the resonance lifetime of the adsorbed molecule, τ, relative to that of the free molecule, τ^0, is

$$\tau = \frac{\tau^0}{(1+\mathrm{Re}\,S)}. \tag{50}$$

This simple model suggests that when a molecule is adsorbed at a surface the lifetime is modified by a factor of

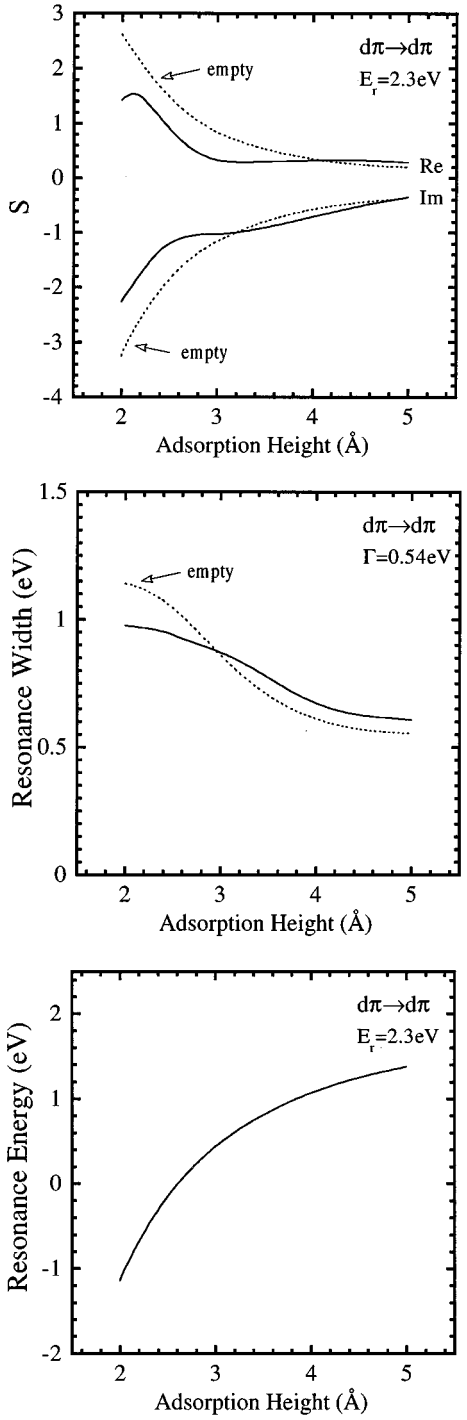

FIG. 10. Upper panel: the real and imaginary parts of the calculated S matrix for $d\pi \rightarrow d\pi$ scattering, plotted as a function of the adsorption height of a molecule above the top site of a Ag(111) substrate. Center panel: The calculated resonance width of $^2\Pi_g$ resonance of N_2 adsorbed perpendicular to a Ag(111) substrate, above the top site. Lower panel: The calculated resonance energy of $^2\Pi_g$ resonance of N_2 adsorbed perpendicular to a Ag(111) substrate, above the top site.

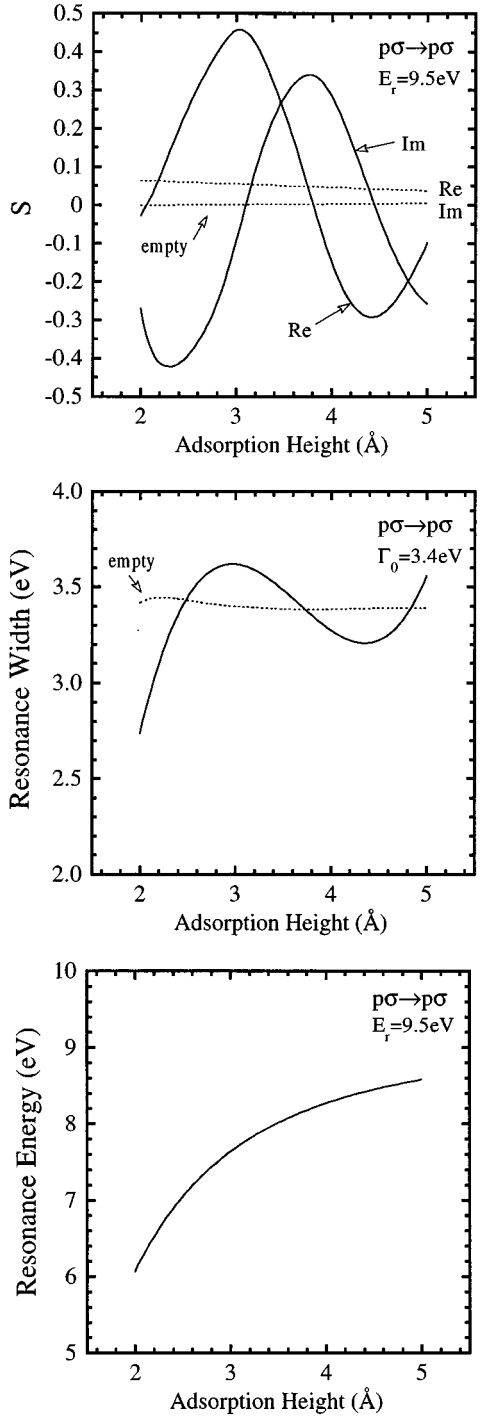

FIG. 11. Upper panel: the real and imaginary parts of the calculated S matrix for $p\sigma \rightarrow p\sigma$ scattering, plotted as a function of the adsorption height of a molecule above the top site of a Ag(111) substrate. Center panel: The calculated resonance width of $^4\Sigma_u^-$ resonance of O_2 adsorbed perpendicular to a Ag(111) substrate, above the top site. Lower panel: The calculated resonance energy of $^4\Sigma_u^-$ resonance of O_2 adsorbed perpendicular to a Ag(111) substrate, above the top site.

$(1+\mathrm{Re}\, S)$. Significantly, this factor depends only upon the real part of the substrate scattering matrix evaluated at the energy of the resonance.

Now consider Figs. 8 and 9, which display the real part of S as a function of the resonance energy. In the low-energy regime ($E_r \lesssim 2$ eV), the real part of S is positive and increases monotonically as the resonance energy is decreased. According to our simple model, Eq. (50) predicts that the resonance lifetime would decrease monotonically as the resonance energy decreases, or equivalently, as the molecule approaches

the substrate. As is shown in Figs. 10 and 11, and discussed earlier in this section, this precise behavior is observed in the computed lifetime of the $^2\Pi_g$ (2.3 eV) state of N_2 physisorbed on Ag(111), Fig. 10. In the higher-energy regime, Fig. 11 shows that Re S oscillates. This behavior is observed in the lifetime of the $^4\Sigma_u^-$ (9.5 eV) state of O_2, also shown in Fig. 11. Note the qualitative correspondence between the oscillatory structure of Re S and the calculated lifetime shown in Figs. 10 and 11.

IV. CONCLUSIONS

In this paper we have presented the computational and theoretical details of a new approach to the calculation of the lifetime, energy, and cross sections for negative-ion formation in adsorbed molecules. This theory is based upon a layer-KKR treatment of electron scattering in the substrate. This method allows the treatment of the substrate electronic structure and its effect upon the lifetime and energy of adsorbate negative ions. Applications of this approach to specific molecule-surface systems may be found elsewhere.[30–34]

Our present approach has a number of limitations which we will now discuss. Perhaps the most serious limitation of the present theory is the neglect of the modification of the molecular core potential by the substrate. This is a reasonable approximation for physisorbed molecules, but is less accurate for strongly chemisorbed species, where charge transfer occurs between the molecule and the substrate. A related issue is the role of the polarization potential, which is known to have an important influence upon the formation of some resonant states in free atoms and molecules. For a molecule adsorbed at a metallic surface, the long-range polarization potential is screened but in the present model, and all prior calculations for adsorbed molecules, any modification of the molecular polarization potential by the substrate is neglected. This assumption can be partially justified by noting that only when the probe electron is far from the adsorbed molecule is the polarization potential strongly altered by the presence of the image dipole. However, in this case, the long-range interaction potential of the probe electron with the surface-molecule system is dominated by a lower-order multipole moment, the (monopole) image screening of the probe electron by the substrate.

The limitations of the present implementation of the layer-KKR method described in this paper could be alleviated by including the appropriate density-functional representation of the electron-electron interaction and by computing self-consistent electronic potentials for the electron-molecule-substrate interaction. We are currently working on this problem. In the meantime, applications of the layer-KKR theory will be confined to calculation of the resonance behavior of physisorbed or weakly chemisorbed molecules at metallic surfaces.

ACKNOWLEDGMENTS

This research was supported by the National Science Foundation, Division of Materials Research, Grant No. DMR-9319436. We acknowledge the donors of the Petroleum Research Fund, administered by the American Chemical Society, and NATO for partial support of this work.

[1] R. E. Palmer and P. J. Rous, Rev. Mod. Phys. **64**, 383 (1992).
[2] R. E. Palmer, Prog. Surf. Sci. **41**, 51 (1992).
[3] L. Sanche, J. Phys. B **23**, 1597 (1990).
[4] L. Sanche, Comm. At. Mol. Phys. **26**, 321 (1991).
[5] J. Gadzuk, Annu. Rev. Phys. Chem. **39**, 395 (1988).
[6] D. Schmeisser, J. Demuth, and P. Avouris, Phys. Rev. B **26**, 1457 (1982).
[7] J. Gadzuk, J. Chem. Phys. **79**, 3982 (1983).
[8] E. Jensen, P. J. Rous, and R. Palmer, Surf. Sci. **237**, 153 (1990).
[9] P. J. Rous and R. W. R. E. Palmer, Phys. Rev. B **41**, 4793 (1990).
[10] R. E. Palmer, P. J. Rous, J. Wilkes, and R. F. Willis, Phys. Rev. Lett. **60**, 329 (1988).
[11] P. J. Rous, R. F. Willis, and R. E. Palmer, Phys. Rev. B **39**, 7552 (1989).
[12] E. Jensen, R. Palmer, and P. J. Rous, Phys. Rev. Lett. **64**, 1301 (1990).
[13] E. Jensen, R. Palmer, and P. J. Rous, Chem. Phys. Lett. **169**, 204 (1990).
[14] R. Ramsier and J. Yates, Surf. Sci. Rep. **12**, 243 (1991).
[15] J. Gadzuk, L. J. Richter, and S. A. Buntin, Surf. Sci. **235**, 317 (1990).
[16] X.-L. Zhou, X.-Y. Zhu, and J. White, Surf. Sci. Rep. **13**, 73 (1991).
[17] S. M. Harris, S. Holloway, and G. R. Darling, J. Chem. Phys. **102**, 8235 (1995).
[18] P. Haochang, T. Horn, and A. Kleyn, Phys. Rev. Lett. **57**, 3035 (1986).
[19] A. Kleyn, Vacuum **41**, 248 (1990).
[20] S. Holloway and J. Gadzuk, J. Chem. Phys. **82**, 5203 (1985).
[21] P. van der Hoek and E. Baerands, Surf. Sci. Lett. **221**, L791 (1989).
[22] G. Schultz, Rev. Mod. Phys. **45**, 378 (1973).
[23] G. Schultz, Rev. Mod. Phys. **45**, 423 (1973).
[24] L. Sanche and M. Michaud, Chem. Phys. Lett. **84**, 497 (1981).
[25] L. Sanche and M. Michaud, Phys. Rev. B **30**, 6078 (1984).
[26] A. Gerber and A. Herzenberg, Phys. Rev. B **31**, 6219 (1985).
[27] D. Teillet-Billy and J. Gauyacq, Nucl. Instrum. Methods **58**, 393 (1991).
[28] D. Teillet-Billy, V. Djamo, and J. Gauyacq, Surf. Sci. **269/270**, 425 (1992).
[29] P. J. Rous, Surf. Sci. **341**, 213 (1995).
[30] D. Hartley and P. J. Rous, Surf. Sci. **341**, 213 (1995).
[31] P. J. Rous and D. Hartley, Chem. Phys. Lett. **236**, 299 (1995).
[32] P. J. Rous, Surf. Sci. **326**, 67 (1995).
[33] P. J. Rous, Surf. Sci. **334**, 318 (1995).
[34] P. J. Rous, Phys. Rev. Lett. **74**, 1835 (1995).
[35] J. Gadzuk, Surf. Sci. **342**, 345 (1995).
[36] J. Davenport, W. Ho, and J. Schrieffer, Phys. Rev. B **17**, 3115 (1978).
[37] D. Dill and J. Dehmer, J. Chem. Phys. **61**, 692 (1974).
[38] J. Siegel, D. Dill, and J. Dehmer, J. Chem. Phys. **64**, 3204 (1976).
[39] C. Noble and P. Burke, Phys. Rev. Lett. **68**, 2011 (1992).
[40] P. Burke and K. Barrington, *Atomic and Molecular Processes: An*

R-Matrix Approach (Institute of Physics, Bristol, 1993).
[41] P. J. Rous, Surf. Sci. Lett. **279**, L191 (1992).
[42] V. Djamo, D. Teillet-Billy, and J. Gauyacq, Phys. Rev. Lett. **71**, 3267 (1993).
[43] P. Nordlander, Phys. Rev. B **46**, 2584 (1992).
[44] J. Maclaren, S. Crampin, and D. Vvedensky, Phys. Rev. B **40**, 12 164 (1989).
[45] J. Pendry, *Low Energy Electron Diffraction* (Academic, London, 1974).
[46] R. Jones and P. Jennings, Surf. Sci. Rep. **9**, 165 (1988).
[47] E. McRae, Rev. Mod. Phys. **51**, 541 (1979).
[48] R. Jones, P. Jennings, and O. Jepsen, Phys. Rev. B **29**, 6472 (1984).
[49] N. Smith, C. Chen, and M. Weinert, Phys. Rev. B **40**, 7565 (1989).
[50] K. Kambe, Z. Naturforsch. Teil A **22**, 442 (1967).
[51] K. Kambe, Z. Naturforsch. Teil A **22**, 322 (1967).
[52] K. Kambe, Z. Naturforsch. Teil A 1280 (1968).
[53] S. Cunningham, Phys. Rev. B **10**, 4988 (1974).